Materials Chemistry and Physics 344 (2025) 131137

Contents lists available at ScienceDirect

Materials Chemistry and Physics

journal homepage: www.elsevier.com/locate/matchemphys

Enhanced relaxation dynamics in silver-doped chitosan nanocomposites: Probing the charge carrier dynamics and terahertz dielectric response

Can Koral [a,d,*], Michela Marsico [b], Zahra Mazaheri [c,d], Gian Paolo Papari [c,d], Antonello Andreone [c,d], Roberto Teghil [b], Angela De Bonis [b]

[a] Department of Health Sciences, University of Basilicata, 85100, Potenza, Italy
[b] Department of Basic and Applied Sciences, University of Basilicata, 85100, Potenza, Italy
[c] Department of Physics "E. Pancini", University of Naples "Federico II", 80126, Napoli, Italy
[d] National Institute for Nuclear Physics, Division of Naples, 80126, Napoli, Italy

HIGHLIGHTS

- THz Spectroscopy reveals dielectric changes in chitosan-Ag.
- Drude-Smith & Havriliak-Negami models elucidate relaxation dynamics in chitosan composite.
- Ag NPs modify the local electric field in chitosan.
- Ag NPs alter electro-optical properties of chitosan films.

ABSTRACT

This study investigates the influence of silver nanoparticle incorporation on the electro-optical properties of chitosan, a biocompatible and versatile polymer with promising applications in biomedicine, energy storage, and sensing technologies, to name a few. Silver nanoparticles were synthesized by nanosecond laser ablation of the silver target in the polymeric solution. Terahertz time-domain spectroscopy was used to determine the complex dielectric function of pure chitosan and chitosan-silver nanocomposite films over a broad frequency range. The experimental data were analyzed using theoretical models, based on the Drude-Smith and Havriliak-Negami equations, to elucidate the underlying charge carrier dynamics and dielectric relaxation processes. Additionally, complex impedance and complex dielectric modulus analyses were conducted, incorporating Cole-Cole plots. The findings reveal a significant enhancement in the relaxation dynamics of the nanocomposite compared to pure chitosan, evidenced by a shift towards higher frequencies in the imaginary part of the dielectric function and a characteristic quarter-circle arc in the Cole-Cole plot. This study provides valuable insights into the structure-property relationships governing the electro-optical behavior of chitosan-based nanocomposites, paving the way for their tailored design and optimization for advanced technological applications.

1. Introduction

The terahertz regime, situated between electronics and photonics, holds immense potential for applications ranging from high-speed communication and non-destructive imaging to sensing and spectroscopy [1–3]. However, this potential can be fully realized only by developing materials with tailored properties in this unique frequency range. Nanoparticle-embedded polymers have emerged as promising candidates, offering a versatile platform to engineer dielectric properties and manipulate THz wave interactions [4]. Chitosan (CT) has garnered significant attention due to its exceptional properties, including high biocompatibility, biodegradability, low toxicity, and inherent proton conductivity, as well as its ability to form flexible, transparent films [5, 6] including the development of sustainable and environmentally friendly materials for flexible electronic applications, such as biopolymer composites based on chitosan and polyvinyl alcohol [7].

. Previous research has focused on the biomedical applications of CT and CT-based composites [8–11], such as the curative effect on wounds, the useful effects on skin, and the ability to remove mercury and cadmium from solutions [12–15]. Similarly, incorporating nanofillers like nanocurcumin, grape seed extract, chicory extract, aluminum oxyhydroxide, and nickel oxide offers a versatile approach to tailoring the properties of chitosan composites. [16–18]. Various approaches also include hybrid approaches such as the use of Chitosan/Phosphosilicate/Al2O3 [19] or Gelatin-Mg3Si2O54 nano-composites [20].

Recent examples demonstrate the modification of permittivity

---

* Corresponding author.
E-mail address: can.koral@unibas.it (C. Koral).

https://doi.org/10.1016/j.matchemphys.2025.131137
Received 24 March 2025; Received in revised form 5 June 2025; Accepted 8 June 2025

(silver-modified chitosan-corn starch-SiO2) [21], conductivity (Fe2O3@NiO in Chitosan-PEG) [22], optical properties (Aminopropyltriethoxysilane-SiO2 with carbon nanotubes) [23], and THz absorbance (Copper Doped Zinc Magnesium Titanate Nanoceramics) [24].

Recently, the growing need for sustainable and efficient energy technologies has also driven extensive investigations into the use of chitosan as a polymer electrolyte in electrochemical devices, fuel cells, batteries, supercapacitors, and sensor technologies [25–28]. Although the conductivity of pure chitosan is often insufficient for practical applications, the electrical properties can be tuned by adjusting the filler concentration, allowing for significant enhancement of insulating polymer conductivity through the incorporation of conductive fillers [29–31].

This study employs terahertz Time Domain Spectroscopy (THz-TDS) to investigate the enhanced relaxation dynamics in silver-doped chitosan nanocomposites, aiming to better understand the influence of the electronic properties and charge transport mechanisms within the CT matrix. By deeply studying the dielectric properties of chitosan enhanced with silver nanoparticles (CT-Ag), we explore the potential of these materials for THz technology applications, including high-speed communication, non-destructive imaging, sensing, and medical diagnostics [5,6].

Ag nanoparticles were synthesized using nanosecond laser ablation in liquid, a technique offering distinct advantages over traditional chemical synthesis methods [32,33]. Intense laser pulse irradiation of a solid target results in the formation of laser-induced plasma. In laser ablation in liquid experiments, the medium tightly confines the plasma, resulting in the formation of a cavitation bubble with oscillating dynamics. Within this cavitation bubble, the nucleation and growth of nanoparticles occur. Upon bubble collapse, the nanoparticles are released into the surrounding liquid. This technique produces high-purity nanoparticles without requiring stabilizing agents or reducing chemicals. Moreover, laser ablation in liquid is environmentally friendly, as it generates minimal chemical waste and avoids the use of toxic substances. These advantages make it an ideal method for producing nanoparticles for applications in sensitive environments, such as biomedical and sensing technologies, where purity and precise control over particle characteristics are essential. By incorporating silver nanoparticles produced via laser ablation in liquid, this study not only optimizes the dielectric properties of CT-Ag composites for THz applications but also enhances the material's sustainability and safety profile. This approach further supports the development of advanced materials that are both effective and environmentally responsible, aligning with the growing demand for green synthesis techniques in nanotechnology.

To interpret the observed dielectric response, we employed several theoretical models and analysis techniques. After extracting the dielectric function of the CT and the CT-Ag composite, we used the Drude-Smith (DS) equation to describe the frequency-dependent conductivity of the samples, providing insights into the dynamics of free and bound charge carriers. Moreover, we employed the Havriliak-Negami (HN) equation to model the complex dielectric function, accounting for the distribution of relaxation times often present in heterogeneous materials like polymer composites. From the outcome of the initial analysis, we further investigated the complex impedance and dielectric modulus analysis to gain deeper insights into the electrical relaxation processes taking place in the composites. Finally, to complete and visualize the dielectric response, we utilized Cole-Cole plots, providing a clear graphical representation of the dielectric data and facilitating the analysis of relaxation processes and impedance characteristics.

By combining the results obtained from THz-TDS measurements with insights derived from the Drude-Smith, Havriliak-Negami and Cole-Cole analyses, in correlation with the complex impedance and the complex dielectric modulus analysis, we aim to elucidate the underlying physics governing the electron transport and electro-optical properties of chitosan and its nanocomposite counterpart. Our findings reveal that the addition of silver nanoparticles significantly alters the dielectric relaxation behavior, as evidenced by the Cole-Cole plot analysis. This analysis sheds light on the significant role of interfacial effects and the intrinsic properties of silver nanoparticles in governing the electrical relaxation dynamics of the composite material.

2. Materials and methods

2.1. Sample fabrication and characterization

Silver nanoparticles (Ag-NPs) were synthesized by nanosecond laser ablation of an Ag target (Goodfellow, 99.999 %) in a 1 g/L chitosan solution. The solution was prepared by dissolving chitosan (100–300 KDa, deacetylation degree 75 %, Acros Organics) in 0.1 % acetic acid (Sigma-Aldrich, 99.8 %) and stirring at 35 °C for 4 h until fully dissolved. A nanosecond Nd:YAG laser (Handy-YAG – Quanta System) with a wavelength of 532 nm, pulse duration of 7 ns, repetition rate of 10 Hz, and power of 150 mW was used for the ablation experiments. The laser beam was vertically focused on the silver target using a lens with a focal length of 50 mm, obtaining a spot size of 0.8 mm, for a fluence of 1.5 J/cm^2. The target was placed in a beaker containing 50 ml of the chitosan solution, the liquid column was maintained at a height of 2 cm and the ablation lasts for 45 min. The Ag NP concentration was 8 μg/mL, as evaluated weighting the silver target before and after the ablation process. By using these conditions, it is possible to obtain stable colloidal Ag NPs embedded in the polymeric solution, avoiding the polymer degradation during the ablation experiment [34]. 20 ml of the Ag-CT solution was dried at room temperature in a 25 × 25 mm^2 plate to prepare free standing films of the same size and approximate thickness in the orders of 50 μm. Ag NPs are present in the composite films with an amount of 0.8 %ww.

Morphology and size distribution of the Ag NPs were characterized by TEM analysis. Few drops of the colloidal solution were dropped on Holey Carbon copper grids (Agar Scientifics) and observed with a FEI TECNAI G2 F20 instrument operating at 200 kV. Images were analyzed by using the free software ImageJ. ATR-FTIR ALPHA instrument (Bruker) was used to characterize the prepared films. Spectra were acquired in the 400-4000 cm^{-1} range with a resolution of 2 cm^{-1}. XRD diffractogram of the composite was obtained by using a D5000 instrument (Siemens) in a Bragg-Brentano configuration, equipped with a CuKα radiation source, operating at 40 kV, 32 mA, in the 5–60 2θ range.

2.2. Terahertz time domain spectrometer

Terahertz Time Domain Spectroscopy served as the primary experimental technique, enabling us to determine the complex dielectric function of our samples over a broad frequency range (0.2–2.5 THz). TDS transmission measurements were carried out using a femtosecond laser-driven, all-fiber-coupled THz spectrometer (TERAK15, Menlo Systems). Photoconductive antennas were employed for both THz generation and detection, in line with Polymethylpentene (TPX) lenses used to collimate and focus the broad THz frequency range onto the samples. The time-domain signals passing through the sample at normal incidence and the free-space reference were acquired separately and transferred into the frequency domain using a Fast Fourier Transform procedure. The material transfer complex function $\widetilde{T}(\omega)$ was extracted from the ratio of the electric field $E_s(\omega)$ transmitted through the sample and the reference signal $E_r(\omega)$ transmitted in air. The complex index of refraction $\widetilde{n}(\omega) = n(\omega) + ik(\omega)$ was then extracted from the transfer function and used to evaluate the complex dielectric function, $\widetilde{\varepsilon} = \varepsilon' + \varepsilon''$, where $\varepsilon' = n^2 - k^2$ and $\varepsilon'' = 2nk,$ and the absorption coefficient $\alpha = 2\omega k/c$.

The dielectric response of the mixture was obtained from the frequency domain analysis using an algorithm that iteratively minimizes the distinct peaks arising from the multiple reflections inside the sample due to periodic Fabry–Perot oscillations [35]. The same algorithm precisely determined the thickness by applying an additional Fourier transform to the frequency domain data, which generates information in a quasi-space domain allowing the actual sample thickness to be precisely determined [36]. The normalized quasi-space peaks plotted as a function of thickness revealed clear minima at 36 μm for the CT film and 46 μm for the silver-nanoparticle doped chitosan film [37]. This measurement, with an associated ±1 μm uncertainty, was considered in the error analysis of the complex refractive index and complex dielectric function.

2.3. *Model fitting procedure*

The fitting of all models employed in this analysis was performed using a custom non-linear regression algorithm implemented in MATLAB. The algorithm utilizes the Levenberg-Marquardt method to optimize model parameters and minimize the error between theoretical predictions and measured values. The Levenberg-Marquardt algorithm is particularly well-suited for non-linear least-squares problems, offering a balance between the steepest descent and Gauss-Newton methods to efficiently converge towards optimal parameter values. This custom implementation provided flexibility in adapting the fitting procedure to the specific characteristics of the models and datasets.

3. Results and discussion

3.1. *Chitosan + Ag NPs composite characterization*

Size and morphology of Ag NPs obtained by laser ablation of a silver target in the polymeric solution were investigated by TEM analysis(see Fig. 1). Well dispersed spherical Ag NPs were obtained, characterized by a mean Feret diameter of 14 nm and an aspect ratio of 1.1.

ATR-FTIR analysis allows to highlight the interaction between AgNPs and the polymer. In Fig. 2 vibrational spectra of Chitosan and Chitosan + AgNPs films are reported. In both spectra are present the broad band between 3600 and 3000 cm^{-1} due to the stretching of the O–H and N–H bonds, the band centered at 2800 cm^{-1} due to the stretching vibration of the C–H groups and the signals at about 1670, 1580 and 1315 cm-1, related to the stretching of C═O bonds in amide II, to the bending of N–H of amide II and to the C–N stretching of amide III, respectively. The observed decreasing of the band at 1580 cm^{-1} for the Chitosan + AgNPs film suggests the interaction of the metallic nanoparticles with the amino groups of the polymer [38,39].

The XRD diffractogram of Chitosan + AgNPs film shows two bands at about 10° and 20° that can be assigned to (020) and (200) reflections of chitosan, respectively [40] and a low intensity peak at 38,2°, that can be assigned to the (111) planes of silver in the FCC crystal structure (JCPDS card no. 87–0720).

3.2. *THz frequency domain analysis*

The complex index of refraction and the absorbance plots of the samples under test are given in Fig. 3(a) and (b) respectively.

The measured values of the complex index of refraction and absorbance are in line with previously reported data for similar materials [41].The scattered points at around 1.1, 1.8, 1.9, 2.0, and 2.5 THz correspond to water vapour absorption peaks, which are inherent to THz time-domain spectroscopy measurements performed under ambient conditions. The raw frequency-domain plots include these data points, but they have been removed from the modelled complex dielectric function to enhance visual clarity and facilitate interpretation of the underlying dielectric response. This removal does not affect the analysis or conclusions.

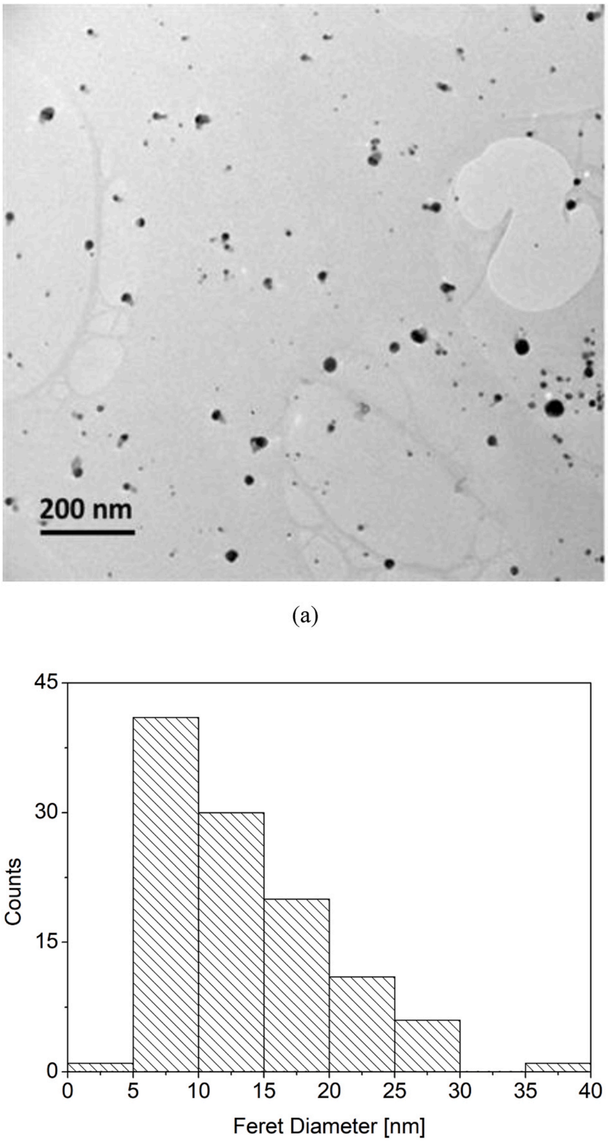

(a)

(b)

Fig. 1. (a) TEM micrograph illustrating the morphology and dispersion of silver nanoparticles within the chitosan matrix of the CT + AgNP composite. (b) Size distribution histogram of the AgNPs, revealing a mean Feret diameter of 14 nm and an aspect ratio of 1.1.

3.3. *Drude-Smith model*

The THz frequency range corresponds to the typical timescales of carrier scattering events in materials, allowing the direct study of charge carrier dynamics, including the effects of localization, by probing materials with THz radiation. The Drude-Smith (DS) model is a suitable choice for analyzing the chitosan-silver nanoparticle system at terahertz frequencies [42,43]. It accounts for the potential localization of charge carriers due to the nanoscale dimensions of the particles and the influence of the CT matrix. By fitting the DS model to the experimental data, we extracted valuable information about the charge transport properties of the composite material, such as the degree of localization and the scattering rate of charge carriers [44,45,48].

Nanomaterials have often dimensions comparable to the mean free path of electrons, making them more susceptible to scattering off boundaries and interfaces rather than other electrons or lattice vibrations. This scattering behavior leads to localized charge carriers, which

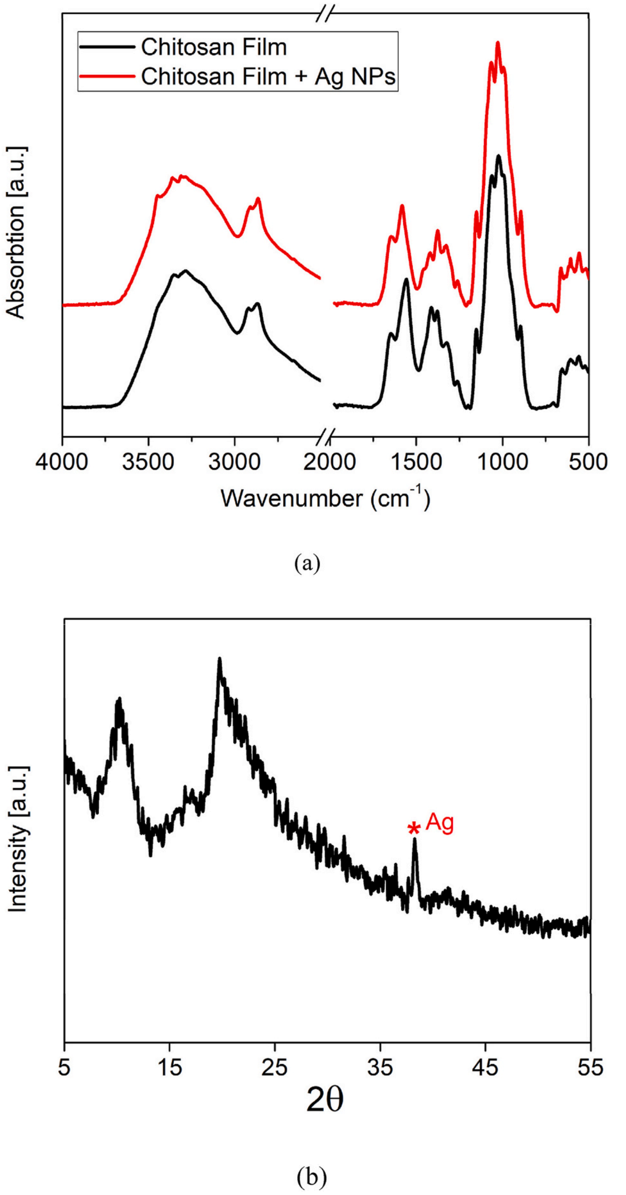

(a)

(b)

Fig. 2. (a) ATR-FTIR spectra of chitosan and Chitosan + AgNP films, showing characteristic vibrational bands. The decrease in the 1580 cm-1 band for the composite indicates interaction between AgNPs and the amino groups of chitosan. (b) XRD diffractogram of the Chitosan + AgNP film, revealing chitosan reflections at 10° and 20° and a silver peak at 38.2° (shown with a star).

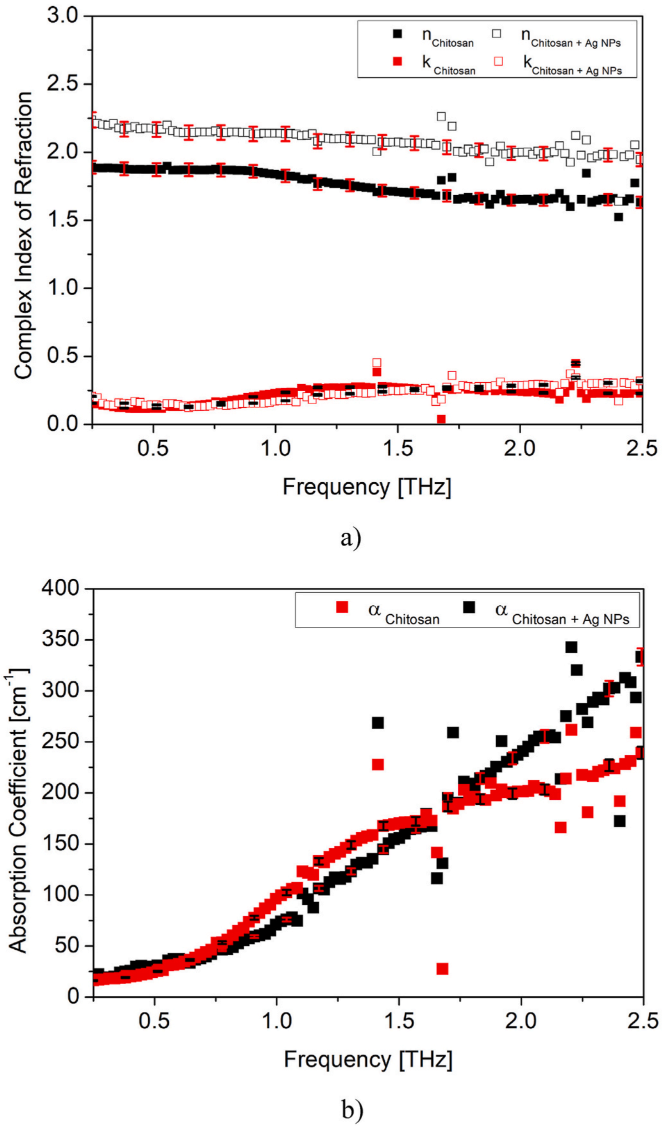

a)

b)

Fig. 3. (a) Complex refractive index and (b) absorbance of the pure CT film and silver nanoparticle-doped CT film, as extracted from THz-TDS transmission measurements. Error bars represent ±1 μm uncertainty in thickness measurements plot with contrasting colors to improve visibility. (For interpretation of the references to color in this figure legend, the reader is referred to the Web version of this article.)

do not move freely throughout the material. The DS model is an extension of the classical Drude model, which assumes completely free electrons. The key difference is the inclusion of the phenomenological backscattering parameter c_1, ranging between 0 and -1, which accounts for the persistence of velocity after a collision. A negative value indicates a higher probability of backscattering, characteristic of localized carriers in nanomaterials [46–50].

Within the DS model the dielectric function $\tilde{\varepsilon}(\omega)$ of a nanomaterial system can be well described under the single-scattering approximation using the following formula:

$$\tilde{\varepsilon}(\omega) = \varepsilon_\infty - \left\{ \frac{\omega_p^2}{\omega^2 + i\omega\omega_\tau}\left(1 + c_1\frac{\omega_\tau}{\omega_\tau - i\omega}\right)\right\} \tag{1}$$

where ε_∞ is the background permittivity, $\omega = 2\pi\nu$ is the radial frequency, $\omega_\tau = 1/\tau$ is the relaxation frequency (τ is the carrier collision time) and ω_p is the plasma frequency. c_1 accounts for the fraction of charge carriers' initial velocity retained after one collision only. The corresponding complex conductivity can be obtained using the expression: $\tilde{\sigma}(\omega) = -i[\tilde{\varepsilon}(\omega) - \varepsilon_\infty]\varepsilon_0\omega$, where ϵ_0 is the free space permittivity. The Drude-Smith model fit to the complex dielectric function is shown in Fig. 4(a) and (b), for the pure CT film and the silver nanoparticle-doped CT composite film respectively.

Fig. 4 shows a nice matching between fits provided using Eq. (1) and the experimental data for both the CT and CT-Ag composite materials, demonstrating the model capacity to account for the localization of charge carriers.

The corresponding analysis provides several key insights into the impact of incorporating silver nanoparticles into the CT composite. Firstly, the higher plasma frequency observed in the composite suggests either a greater concentration of mobile charge carriers or enhanced charge carrier mobility, which can be attributed to the addition of the silver nanoparticles. Furthermore, the composite exhibits a shorter scattering time, indicating that charge carriers experience more scat-

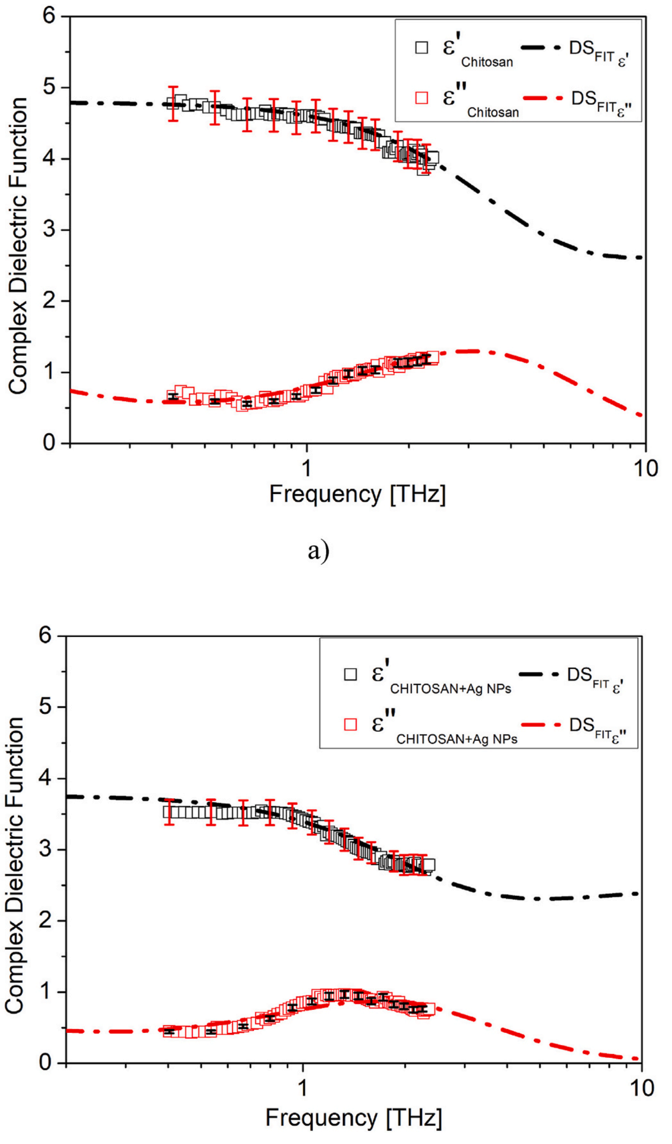

a)

b)

Fig. 4. Drude-Smith model fits to the complex dielectric function of (a) the pure chitosan film and (b) the silver nanoparticle-doped chitosan composite film. The real (ε′) and imaginary (ε") components of the dielectric function are shown as a function of frequency. Experimental data are represented by red and black squares for the real and imaginary components, respectively. The corresponding Drude-Smith fits are shown as dash-dotted lines, following the same color scheme. Error bars represent ±1 μm uncertainty in thickness measurements plot with contrasting colors to improve visibility. (For interpretation of the references to color in this figure legend, the reader is referred to the Web version of this article.)

tering events due to the presence of the silver nanoparticles within the CT matrix. Additionally, the confinement parameter $c_1 \approx -1$ indicate that the charge carriers are fully localized for both the pure CT and the composite material. Lastly, the higher value of ε_∞ in the composite suggests a greater contribution from fast polarization mechanisms at high frequencies, which could be attributed to the influence of the Ag NPs. The DS fitting parameters are given in Table 1.

While precise error quantification for the fitting parameters is not possible due to the lack of statistical data, the Drude-Smith model exhibits excellent agreement with the empirical data, achieving R^2 values greater than 0.95.

Table 1
Drude-Smith model fitting parameters for the pure chitosan film and the silver nanoparticle-doped chitosan composite film.

	ω_p [THz]	ε_∞^{DS}	c_1	ω_τ [THz]
Chitosan	3.4	2.48	−0.99	18.70
Chitosan + Ag NPs	7.5	2.86	−0.99	33.90

The decreased resonance frequency observed in the composite material indicates that the incorporation of silver nanoparticles influences the oscillatory behavior of bound charges within the chitosan matrix when subjected to the electromagnetic field. In other words, the shifts observed in the resonance frequency of the composite material can be understood because of the complex interplay between the silver nanoparticles and the molecular-scale structure of the chitosan matrix, which manifests as alterations to the vibrational response of the material as a whole.

These mechanisms depend strongly on the properties and distribution of the nanoparticles. The observed shifts can be attributed to two primary factors. The first is the potential alteration of the local dielectric environment, wherein the presence of silver nanoparticles introduces interfacial regions and modifies the local dielectric constant surrounding the chitosan molecules. This altered dielectric environment influences the electric field distribution experienced by the bound charges, effectively reducing their restoring force and thus lowering the resonance frequency. The second factor is the modification of the bonding environment, wherein the interaction between silver nanoparticles and chitosan molecules can potentially alter the bonding characteristics within the polymer matrix, such as changes in hydrogen bonding networks, coordination bonds, or other intermolecular interactions [28,30,51–53].

An alternative vision of the transport mechanisms ruling the electrodynamics of the two films may be obtained looking at the comparison between the experimental conductivities and the DS fit results shown in Fig. 5. Here both the real and imaginary term of $\tilde{\sigma}(\omega)$ are plotted.

As already said, the fitting procedure yields for both samples $c_1 = -1$ within the uncertainties of the calculation, which is consistent with the observed frequency behavior for the complex conductivity. Specifically, the real part approaches zero at DC, while the imaginary part is negative. This is interpreted in the DS model as conductivity being dominated by

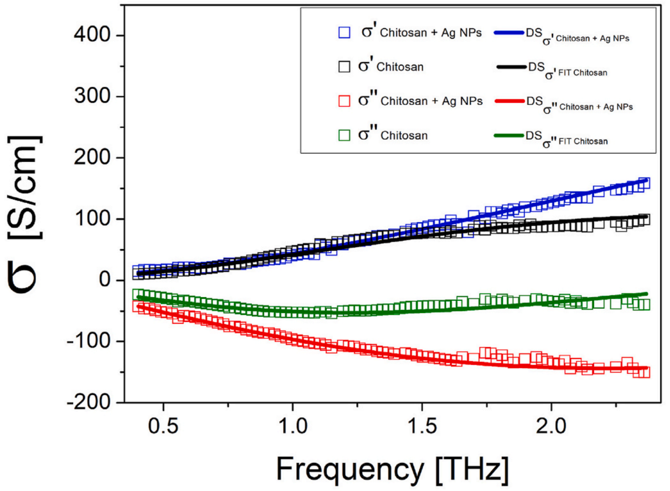

Fig. 5. Complex conductivity of the pure chitosan film and the silver nanoparticle-doped chitosan composite film as a function of frequency. Experimental data are represented by square symbols: black (red) for the real part (σ′) and green (blue) for the imaginary part (σ") of the pure CT (CT-Ag) film. The solid lines represent the corresponding Drude-Smith model fits to the complex conductivity, following the same color scheme. (For interpretation of the references to color in this figure legend, the reader is referred to the Web version of this article.)

carrier backscattering. This suggests that the transport in all samples is dominated by localized charge carriers, consistent with the nanoscale morphology of the samples.

The composite sample exhibits a relatively higher conductivity compared to the pristine chitosan at higher frequencies, indicating that the incorporation of silver nanoparticles enhances the charge transport in the material at these higher frequencies. However, it is important to note that in the studied system the volume fractions of the nanoparticles are below the percolation threshold. Even with the effect of the silver nanoparticles, both systems are behaving like insulators. The observed increase in the absolute values of conductivity can be explained by the high density of structural defects induced by the adopted synthesis conditions, and these defects become more discernible as the wavelengths get closer to the size of the particles or the distance between the charge carriers. Structural defects in chitosan, such as chain ends, entanglements, and crystallinity variations, can be exacerbated by the inclusion of silver nanoparticles, creating interfacial defects. Solution casting, particularly with rapid solvent evaporation, can further trap these defects [51,54,55]. The addition of silver nanoparticles, even at concentrations below the percolation threshold, appears therefore to significantly influence the dielectric properties of the composite material. While the nanoparticles do not induce a transition to a conductive state, they may impact the density and behavior of structural defects within the material, leading to a “nuanced” effect on the dielectric response.

3.4. Havrialik-Negami model

The relatively low conductivity observed within the measured frequency range may suggest that the dielectric relaxation process is the dominant factor, potentially masking any underlying conductive behavior in the material. It is possible that some degree of charge transport exists, but it is overshadowed by the more prominent relaxation phenomena occurring in the system.

The HN model is a generalized dielectric relaxation function that can describe a wide range of polarization phenomena in materials, including those with a distribution of relaxation times [56,57]. It is an empirical modification of the Debye model to account for the broadening (β) and asymmetry (γ) of the dielectric dispersion curve, considering that there is a distribution of relaxation times instead of a single relaxation time and a non-symmetric shape of the dielectric spectrum. Consequently, the HN equation may adequately capture the overall shape of the experimental data without the need to explicitly account for the conductivity contribution.

The Havriliak-Negami equation is expressed as:

$$\widetilde{\varepsilon}(\omega) = \varepsilon_\infty + \frac{\Delta\varepsilon}{\left(1 + (i\omega\tau_{HN})^{\beta}\right)^{\gamma}} \tag{2}$$

where $\Delta\varepsilon$ represents the dielectric relaxation strength (the difference between the low-frequency and high-frequency permittivity), and τ_{HN} is the characteristic relaxation time.

The Havriliak-Negami (HN) equation can describe the frequency dispersion of the dielectric response in a wide range of materials, including polymer composites with nanoscale fillers [56,58]. In a common sense, β and γ are shape parameters, both typically ranging from 0 to 1. β expresses the broadening of the dielectric loss peak, whereas γ provides information on the asymmetry in its shape. When $\beta = \gamma = 1$, the HN equation reduces to the Debye equation, representing a single relaxation process. When $\beta = 1$ and $0 < \gamma < 1$, it becomes the Cole-Davidson equation. When $0 < \beta < 1$ and $\gamma = 1$, it becomes the Cole-Cole equation [59]. Exceeding the typical range of 0–1 for the shape parameters in the HN [56,60]equation suggests complex relaxation processes that depart from standard Debye behaviour.

The Havriliak-Negami model fits to the complex dielectric function are presented in Fig. 6, and the corresponding fitting parameters are summarized in Table 2.

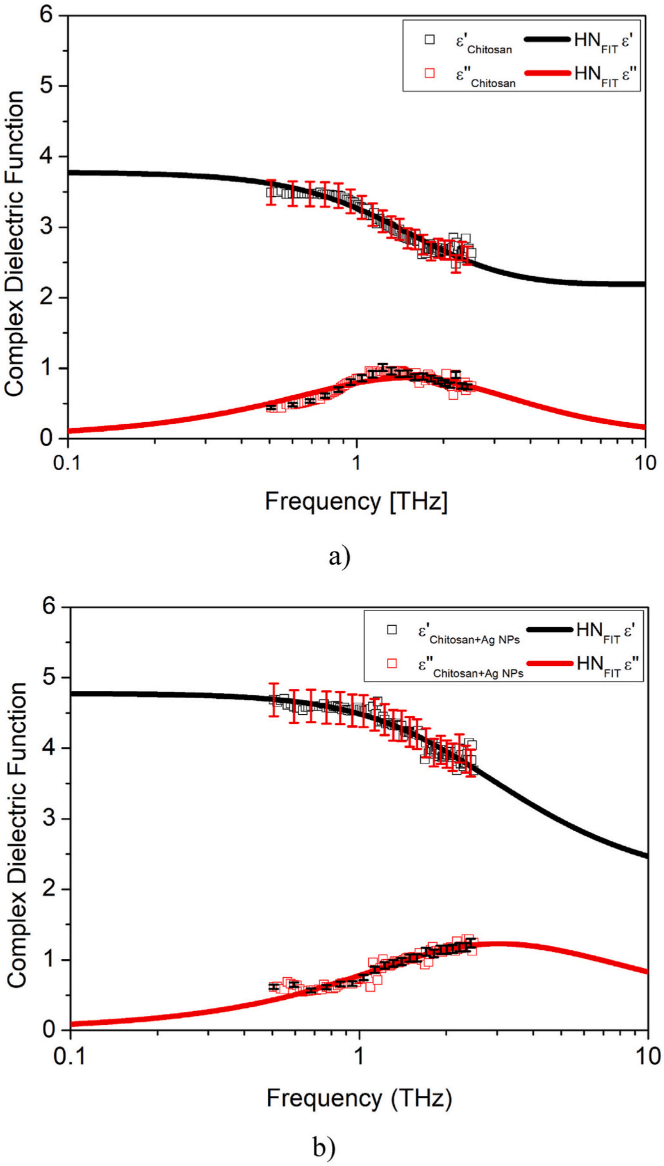

a)

b)

Fig. 6. Havriliak-Negami model fits to the complex dielectric function of (a) the pure chitosan film and (b) the silver nanoparticle-doped chitosan composite film. The real (ε′) and imaginary (ε") components of the dielectric function are shown as a function of frequency. Experimental data are represented by square symbols (black for the real part and red for the imaginary part). The corresponding HN fits are displayed as solid lines. Error bars represent ±1 μm uncertainty in thickness measurements plot with contrasting colors to improve visibility. (For interpretation of the references to color in this figure legend, the reader is referred to the Web version of this article.)

Again, there is an excellent agreement between fitting curve and experimental data, with R^2 values greater than 0.95. This strong correspondence is visually confirmed in Fig. 4, where the HN model effectively captures the key features of the dielectric response, such as the overall shape of the curves and the position of peaks.

Table 2
Havriliak-Negami model fitting parameters for the pure chitosan film and the silver nanoparticle-doped chitosan composite film.

	$\Delta\varepsilon$	β	γ	τ_{HN} [fs]	ε_∞^{HN}
Chitosan	1.75	1.00	1.00	100	2.08
Chitosan + Ag NPs	2.99	0.84	0.82	70	1.85

Data analysis provides several key insights into the impact of incorporating silver nanoparticles into the CT composite. First, the shorter relaxation time τ observed in the composite indicates faster relaxation processes, which aligns with the higher frequency response seen in the Drude-Smith model analysis. This suggests that the silver nanoparticles facilitate or accelerate the relaxation of chitosan dipoles. The shorter relaxation time (τ) observed in the composite indicates faster relaxation processes. This suggests that the silver nanoparticles facilitate or accelerate the relaxation of chitosan dipoles. Additionally, the composite exhibits an increased $\Delta\varepsilon$, implying a larger relaxation strength, likely nanoparticle mediated silver. The ε_∞ value is lower in the composite film, suggesting a reduced contribution from electronic polarization mechanisms at higher frequencies, possibly due to interactions between the silver nanoparticles and the chitosan matrix. The near-unity values of both β and γ for both films indicate near-Debye behaviour with minimal asymmetry in the dielectric loss peak. The decrease in β in the composite suggests a broadening, not narrowing, of the relaxation time distribution, which could be attributed to the heterogeneity introduced by the silver nanoparticles. This heterogeneity could arise from factors such as an inhomogeneous distribution of relaxation times within the material, interfacial polarization effects, or variations in the local environment surrounding the polymer chains due to the presence of the nanoparticles.

In summary, the Havriliak-Negami model offers a flexible, empirical framework to capture the dielectric response, whereas the Drude-Smith model provides a more physically grounded approach. Using a combination of these models and carefully analyzing their parameters one can provide a more comprehensive understanding of the complex dielectric behavior of the chitosan-silver nanoparticle system. The matching of both the Drude-Smith and Havriliak-Negami models with the experimental data may suggest that the chitosan-silver nanoparticle composites exhibit significant charge carrier localization and a distribution of relaxation times, likely due to the complex morphology of the composite, including the interfaces between chitosan and silver nanoparticles.

3.5. *Cole-Cole plots*

To further analyze the dielectric properties of the chitosan and chitosan-silver nanoparticle composite films we analyzed the Cole-Cole (CC) plot of the two samples. The plot displays the imaginary part of the complex permittivity against the real part, and can reveal information about the distribution of relaxation times and the presence of multiple polarization processes [57,61–63]. The CC plots, along with the corresponding high-order polynomial fits, are presented in Fig. 7.

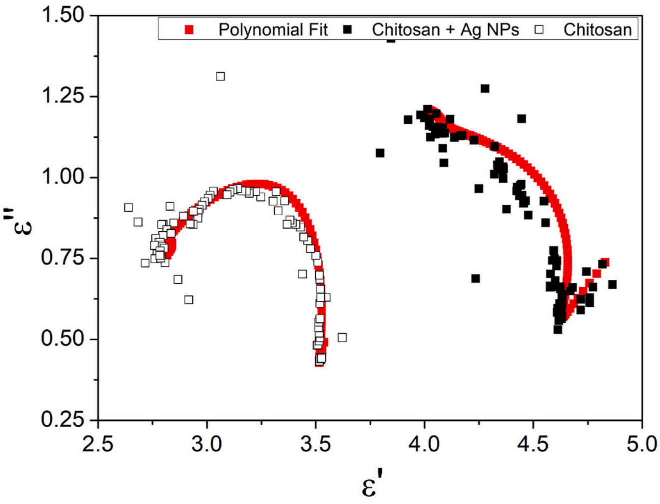

Fig. 7. Cole-Cole plot for the pure chitosan film and the silver nanoparticle-doped chitosan composite film. The imaginary part (ε'') of the complex permittivity is plotted against the real part (ε′). Experimental data for the pure chitosan film are represented by empty black squares, while filled black squares represent the data for the composite film. The corresponding high-order polynomial fits to the data are shown in red. (For interpretation of the references to color in this figure legend, the reader is referred to the Web version of this article.)

The CC plot for pure chitosan exhibits a clockwise semi-circular arc with its center positioned to the left of the positive x-axis. This suggests the material exhibits a relatively Debye-like dielectric relaxation process with a distribution of relaxation times. The presence of a distribution of relaxation times indicates that not all dipoles within the material relax at precisely the same rate. This distribution can lead to a slight deviation from the ideal Debye semicircle, such as a broadening or flattening of the arc. In contrast, the plots for the silver-embedded CT composite show a shift of the arc towards the right side of the axis, forming a quarter-circle with a larger radius. This indicates an increase in the real part of the permittivity at lower frequencies, likely due to the addition of conductive silver nanoparticles enhancing the material's ability to store electrical energy [51]. Furthermore, the change in shape to a quarter-circle and the larger radius suggest a broader distribution of relaxation times in the composite compared to pure CT [64,65]. This could be attributed to the introduction of new interfacial polarization mechanisms at the chitosan-silver boundaries, where the silver nanoparticles, with their free electrons, can accumulate charges at the interfaces, leading to additional polarization effects that contribute to the dielectric response.

In an ideal Debye model, the Cole-Cole plot would form a perfect semi-circular arc centered on the real axis. The fact that in the pure CT film the center of the semi-circle is slightly to the left of the positive real axis suggests a distribution of relaxation times, indicating that the chitosan molecules do not all relax at precisely the same rate [57,59,60,66,67].

In the NP doped sample, instead, the presence of a linear line with a positive slope following the quarter-circle arc in the CC plot suggests an additional conduction mechanism that might imply a significant DC conductivity contribution in the CT-Ag nanocomposite, indicating a pathway for direct current flow through the material due to the presence of the conductive silver nanoparticles. This finding is also consistent with the increase in conductivity observed at higher frequencies from the complex conductivities extracted using the DS model.

Several sources discuss the interpretation of Cole-Cole plots and deviations from ideal Debye behavior. In Refs. [62,63,66] authors provide relevant discussions on Cole-Cole analysis and interpretations. Additionally, information on the relationship between Cole-Cole plots and the distribution of relaxation times can be found in Refs. [59,60,67].

The observed changes in the Cole-Cole plots clearly demonstrate that the incorporation of silver nanoparticles significantly alters the dielectric relaxation behavior of chitosan [51].

Integrating the insights from the Drude-Smith and Havriliak-Negami models provides a cohesive and complementary understanding, while further analysis of the complex modulus and complex impedance offers additional confirmation of the findings [28,56,68].

The broadening of the relaxation time distribution observed in the Havriliak-Negami analysis, indicated by the decrease in β for the chitosan-silver nanocomposite, is further corroborated by the Cole-Cole plots. A deviation from the ideal Debye semicircle, potentially towards a skewed or flattened arc, would visually represent this broadened distribution and suggest a departure from a single relaxation process. Analysis of the complex modulus and impedance data provides complementary insights into the relaxation dynamics. The complex modulus formalism is particularly sensitive to conductivity contributions and interfacial phenomena. A non-Debye response in the complex modulus, such as a broadened or asymmetric peak in the imaginary component (M''), would support the presence of multiple relaxation processes or a distribution of relaxation times within the composite. Similarly, the complex impedance data can reveal information about charge transport mechanisms. A depressed semicircle in the complex impedance plane, or the presence of multiple semicircles, would further indicate the influence of interfacial polarization and the heterogeneous nature of the composite material. These combined analyses provide a comprehensive picture of the enhanced and more complex relaxation dynamics in the silver-doped chitosan nanocomposite compared to pure chitosan.

3.6. Complex impedance and modulus analysis

Analysis of the complex impedance $\widetilde{Z}$ has been widely employed to identify these individual processes, and the data have been analyzed by measuring the complex modulus $\widetilde{M}$, which is the inverse of complex permittivity $\widetilde{\varepsilon}$ and is related to the complex impedance:

$$\widetilde{M}(\omega) = \frac{1}{\widetilde{\varepsilon}\,(\omega)} = M' + jM'' = j\omega C_0\,\widetilde{Z}(\omega) \tag{5}$$

where;

$$M' = \frac{\varepsilon'}{(\varepsilon'^2 + \varepsilon''^2)}, M'' = \frac{\varepsilon''}{(\varepsilon'^2 + \varepsilon''^2)} \text{ and } \widetilde{Z} = Z' + jZ''$$

Here the parameters Z′ and Z’’ represent the resistance and reactance of the material, respectively. The vacuum capacitance C_0 is calculated as $\varepsilon_0 A/d$, where A is the area and d the thickness of the sample space.

The sample thicknesses were estimated using an iterative quasi-space approach, which was described in detail in a previous section, and since the dielectric response was probed using transmitted THz waves the sample surface area A was determined based on the 1 mm spot size of the THz beam.

The complex modulus formalism helps to distinguish the effects of electrode polarization and interfacial phenomena. The imaginary part of the complex modulus plotted against frequency provides insights into the true electrical relaxation processes within the material. In the ideal case, this can be characterized by a conductivity relaxation time. Under such ideal conditions, the peaks in the imaginary part of the complex impedance and complex modulus spectra occur at the same frequency, and their shapes are identical to those predicted by the Debye theory for dielectric loss [69,70]. The imaginary part of the impedance and modulus are plotted in Fig. 8(a) and (b) for the pure chitosan film and the silver nanoparticle-doped chitosan composite film respectively.

The complex modulus analysis reveals that the incorporation of silver nanoparticles into the chitosan matrix leads to significant changes in the electrical relaxation behavior, as they depart from the ideal Debye theory for dielectric loss, even if the predicted response is observed. This deviation suggests that while the CT system exhibits some characteristics consistent with Debye behavior, such as a single relaxation time in certain frequency ranges, the presence of silver nanoparticles introduces additional complexities. One possible explanation for this deviation is the heterogeneous nature of the composite material. The introduction of silver nanoparticles, even below the percolation threshold, can create interfaces between the CT matrix and the nanoparticles [54]. These interfaces can act as trapping sites for charge carriers, leading to a distribution of relaxation times rather than a single relaxation time as predicted by the Debye model [52,55]. This hypothesis is supported by the Havriliak-Negami analysis, which indicates a broadening of the relaxation time distribution in the composite material compared to pure CT.

Furthermore, the silver nanoparticles themselves can contribute to the observed deviation from Debye behavior. The inherent surface charge and potential for aggregation of the nanoparticles can influence the local electric field distribution within the CT matrix. This altered electric field can affect the dipole orientation and relaxation dynamics, leading to deviations from the ideal Debye response. Therefore, the observed departure from Debye behavior in the complex modulus analysis underscores the significant role of both interfacial effects and the intrinsic properties of the silver nanoparticles in influencing the electrical relaxation behavior of the chitosan-silver nanoparticle composite. Another important complementary result we observe from the given plot is the absence of a clear upward trend in the imaginary impedance with increasing frequency within the measured frequency range. This supports the idea that conductivity is not a major contributor in this specific frequency window, which is also consistent with the findings from the Drude-Smith model fits.

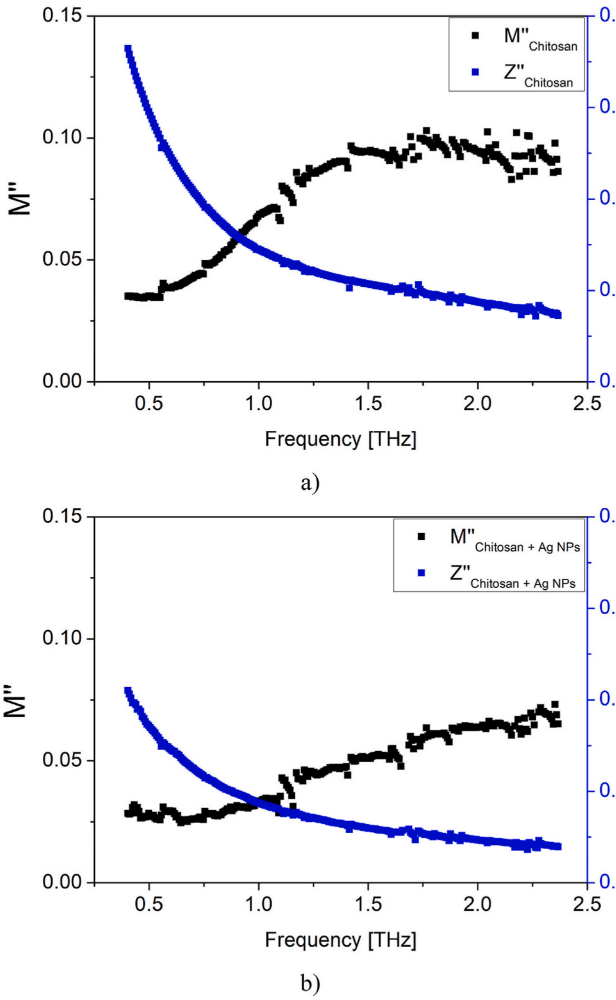

Fig. 8. Frequency dependence of the imaginary part of the complex impedance (Z") and the complex modulus (M") for (a) the pure chitosan film and (b) the silver nanoparticle-doped chitosan composite film. Black squares represent the imaginary part of the modulus (M"), whereas blue squares represent the imaginary part of the impedance (Z"). (For interpretation of the references to color in this figure legend, the reader is referred to the Web version of this article.)

4. Conclusion

The dielectric properties of the chitosan-silver nanoparticle composites were investigated using terahertz time-domain spectroscopy. The obtained data were analyzed adopting different theoretical approaches, specifically the Drude-Smith and the Havriliak-Negami models, and using the Cole-Cole plots and the complex impedance and complex modulus formalisms to provide a comprehensive understanding of the dielectric response in the samples under test.

The Drude-Smith model revealed a significant increase in conductivity at higher frequencies for the composite material compared to pure chitosan, indicating the contribution of the silver nanoparticles to the material's ability to conduct electricity. However, it is important to note that in the studied system, the volume fractions of the nanoparticles are below the percolation threshold, and even with the effect of the silver nanoparticles, both films are behaving like insulators. The observed increase in the absolute values of conductivity can be explained by the high density of structural defects induced by the adopted synthesis conditions, and these defects become more discernible as the wavelengths get closer to the size of the particles or the distance between the charge carriers.

The Havriliak-Negami model analysis reveals key differences in the dielectric relaxation behavior of the chitosan-silver nanocomposite compared to pure chitosan. Both materials exhibit near-Debye behavior, suggested by β and γ values close to unity, however, the composite exhibits enhanced relaxation dynamics, characterized by both a decreased relaxation time (τ) and a broadened distribution of relaxation times (lower β value). This would indicate that the incorporated silver nanoparticles influence the relaxation dynamics by introducing additional relaxation pathways and facilitating faster dipole reorientation within the chitosan matrix. The observed decrease in ε_∞ further indicates that the silver nanoparticles alter the high-frequency dielectric response, likely due to interactions at the chitosan-silver interface.

The Cole-Cole plots provided further insights into the dielectric relaxation behavior. The pure CT exhibited a shape closer to a semicircle, characteristic of a Debye-like relaxation process. However, the composite material showed a distinct deviation from the ideal Debye behavior, with the plot resembling a quarter-circle followed by a linear region. This change in shape suggests a broader distribution of relaxation times in the composite, likely due to the interfacial polarization effects at the chitosan-silver boundaries.

Complex impedance and complex modulus analyses were employed to decouple the various contributions to the dielectric response. The complex modulus analysis highlighted the significant changes in the electrical relaxation behavior upon the incorporation of silver nanoparticles. While the chitosan system exhibited some characteristics consistent with Debye behavior, the composite material showed a clear departure from this ideal model. This deviation was attributed to the heterogeneous nature of the composite and the influence of the silver nanoparticles on the local electric field distribution. The absence of a clear upward trend in the imaginary impedance with increasing frequency further supported the findings from the Drude-Smith model, indicating that conductivity is not a dominant factor in the measured frequency range. Overall, the results demonstrate that the incorporation of silver nanoparticles into a CT matrix significantly alters the dielectric properties and relaxation behavior of the material. The observed changes are attributed to a combination of factors, including the increased conductivity due to the silver nanoparticles, the introduction of interfacial polarization effects, and the influence of the nanoparticles on the local electric field distribution. These findings highlight the potential of chitosan-silver nanoparticle composites for various terahertz technology applications requiring precise control over dielectric properties. These include devices, flexible electronics, polymer electrolytes in electrochemical devices, supercapacitors, and sensor technologies. To further refine our understanding, future studies will employ imaging-based techniques and mean-field theories to map concentration-dependent electro-optical parameter alterations, enabling a more quantitative assessment of the AgNP influence on the composite's dielectric behaviour.

CRediT authorship contribution statement

Can Koral: Writing – review & editing, Writing – original draft, Visualization, Validation, Software, Methodology, Investigation, Formal analysis, Data curation, Conceptualization. **Michela Marsico:** Writing – review & editing, Validation, Investigation, Formal analysis. **Zahra Mazaheri:** Writing – review & editing, Validation, Software, Formal analysis, Data curation. **Gian Paolo Papari:** Writing – review & editing, Validation, Formal analysis, Data curation. **Antonello Andreone:** Writing – review & editing, Validation, Supervision, Resources. **Roberto Teghil:** Writing – review & editing, Validation, Supervision. **Angela De Bonis:** Writing – review & editing, Writing – original draft, Validation, Resources, Funding acquisition, Conceptualization.

Declaration of generative AI and AI-assisted technologies in the writing process

During the preparation of this work the author(s) used [Jenni.Ai] in order to improve language and readability. After using this tool/service, the author(s) reviewed and edited the content as needed and take(s) full responsibility for the content of the publication.

Funding sources

This study was supported by the European Union under the Italian National Recovery and Resilience Plan (NRRP) of NextGenerationEU, in the Frame of the "Missione 4 Componente 2 Investimento 1.4" –SUDELBAT project (CN00000023 – CUP: D43C22001180001), "Centro Nazionale per la Mobilità Sostenibile (MOST)" CN4 Spoke13, and in the partnership on "Telecommunications of the Future" (PE00000001 - program "RESTART").

Declaration of competing interest

The authors declare that they have no known competing financial interests or personal relationships that could have appeared to influence the work reported in this paper.

ABBREVIATIONS

CT: Chitosan, THz: Terahertz, TDS: Time Domain Spectroscopy, NP: Nanoparticles, CC plot: Cole-Cole plot, HN: Havriliak Negami, DS: Drude Smith.

Data availability

Data will be made available on request.

References

[1] C. Koral, et al., Multi-Pass free electron laser assisted spectral and imaging applications in the Terahertz/Far-IR range using the future superconducting electron source BriXSinO, Front. Physiol. 10 (March) (2022) 1–18, https://doi.org/10.3389/fphy.2022.725901.

[2] A. Leitenstorfer, et al., The 2023 terahertz science and technology roadmap, J. Phys. Appl. Phys. (2023), https://doi.org/10.1088/1361-6463/acbe4c.

[3] S.S. Dhillon, et al., The 2017 terahertz science and technology roadmap, J. Phys. Appl. Phys. (2017), https://doi.org/10.1088/1361-6463/50/4/043001.

[4] P.P. Pandey, Silver-based plasmonic nanoparticles and their application as biosensor, J. Polym. Sci. Eng (2023), https://doi.org/10.24294/jpse.v6i1.2405.

[5] A. Pellis, G.M. Guebitz, G.S. Nyanhongo, Chitosan: sources, processing and modification techniques, Gels (2022), https://doi.org/10.3390/gels8070393.

[6] I. Aranaz, et al., Chitosan: an overview of its properties and applications, Polymers (2021), https://doi.org/10.3390/polym13193256.

[7] P. S. MT Ramesan , AC Labeeba Abdulla, Ayisha Jemshiya Kalladi, "Impact of nanocurcumin on mechanical, optical and electrical properties of chitosan/polyvinyl alcohol blend nanocomposites for sustainable applications", doi: https://doi.org/10.1177/0892705724123.

[8] W. Wang, et al., Chitosan derivatives and their application in biomedicine, Int. J. Mol. Sci. (2020), https://doi.org/10.3390/ijms21020487.

[9] N. Desai, et al., Chitosan: a potential biopolymer in drug delivery and biomedical applications, Pharmaceutics (2023), https://doi.org/10.3390/pharmaceutics15041313.

[10] F. Croisier, C. Jérôme, Chitosan-based biomaterials for tissue engineering, Eur. Polym. J. (2013), https://doi.org/10.1016/j.eurpolymj.2012.12.009.

[11] B.A. Alimi, S. Pathania, J. Wilson, B. Duffy, J.M.C. Frias, Extraction, quantification, characterization, and application in food packaging of chitin and chitosan from mushrooms: a review, Int. J. Biol. Macromol. (2023), https://doi.org/10.1016/j.ijbiomac.2023.124195.

[12] Z. Pishgahi, M.R. Nadoshan, M.P. Shotorbani, B. Ghalandari, The effect of using chitosan and β-cyclodextrin on oxidation stability and removal of heavy metals in

minced meat of (Scomberomorus commerson) during refrigeration, J. Food Sci. Technol. (2022), https://doi.org/10.52547/fsct.19.123.105.
[13] M.F. Hamza, Y. Wei, A. Benettayeb, X. Wang, E. Guibal, Efficient removal of uranium, cadmium and mercury from aqueous solutions using grafted hydrazide-micro-magnetite chitosan derivative, J. Mater. Sci. (2020), https://doi.org/10.1007/s10853-019-04235-8.
[14] G. de V. Brião, J.R. de Andrade, M.G.C. da Silva, M.G.A. Vieira, Removal of toxic metals from water using chitosan-based magnetic adsorbents. A Review, Environ. Chem Lett. (2020), https://doi.org/10.1007/s10311-020-01003-y.
[15] R.N. Bharagava, Emerging eco-friendly Green Technologies for Wastewater Treatment, 2020.
[16] M.T. Ramesan, A.J. Kalladi, A.C. Labeeba Abdulla, P. Sunojkumar, B.K. Bahuleyan, Development of biopolymer composite films based on chicory extract reinforced polyvinyl alcohol/chitosan blend via green approach for flexible optoelectrical devices, J. Appl. Polym. Sci. (2024), https://doi.org/10.1002/app.55154.
[17] K. Meera, M.T. Ramesan, Modulating the properties of carboxymethyl chitosan/polyethylene oxide nanocomposites with aluminium oxy hydroxide: a comprehensive study, Int. J. Biol. Macromol. (2024), https://doi.org/10.1016/j.ijbiomac.2024.137034.
[18] O.M. Hunais, T.A. Ramseena, K. Meera, B.K. Bahuleyan, M.T. Ramesan, Tuning the structural, mechanical, thermal and electrical properties of in-Situ polymerized Polyindole/Carboxymethyl Chitosan/Nickel oxide blend nanocomposites for energy storage applications, J. Polym. Environ. (2024), https://doi.org/10.1007/s10924-024-03250-4.
[19] A.M. El Nahrawy, A.M. Mansour, A.B. Abou Hammad, R.S. Ibrahim, A. M. Abouelnaga, M.S. Abdel-Aziz, Optical, functional impact and antimicrobial of Chitosan/Phosphosilicate/Al2O3 nanosheets, J. Inorg. Organomet. Polym. Mater. (2020), https://doi.org/10.1007/s10904-020-01469-x.
[20] A.M. Mansour, A.B. Abou Hammad, A.O. Balkhtb, T.M. Elhelali, A.M. Abouelnaga, A.M. El Nahrawy, Chitosan/In situ Gelatin-Mg3Si2O5(OH)4 nanocomposites via Sol–Gel method: preparation, characterization and antimicrobial properties, Arabian J. Sci. Eng. (2024), https://doi.org/10.1007/s13369-023-07935-1.
[21] A.B. Abou Hammad, A.A. Al-esnawy, A.M. Mansour, A.M. El Nahrawy, Synthesis and characterization of chitosan-corn starch-SiO2/silver eco-nanocomposites: exploring optoelectronic and antibacterial potential, Int. J. Biol. Macromol. (2023), https://doi.org/10.1016/j.ijbiomac.2023.126077.
[22] A.M. Abouelnaga, A.M. Mansour, A.B. Abou Hammad, A.M. El Nahrawy, Optimizing magnetic, dielectric, and antimicrobial performance in chitosan-PEG-Fe2O3@NiO nanomagnetic composites, Int. J. Biol. Macromol. (2024), https://doi.org/10.1016/j.ijbiomac.2024.129545.
[23] A.M. Mansour, A.B.A. Hammad, A.M.E. Nahrawy, Study on optical of Chitosan-Aminopropyltriethoxysilane-SiO2 nanocomposite decorated with carbon nanotubes, Silicon (2024), https://doi.org/10.1007/s12633-023-02661-7.
[24] A.M. El Nahrawy, A.M. Mansour, A.M. Bakr, A.B. Abou Hammad, Terahertz and UV–VIS spectroscopy evaluation of copper doped zinc magnesium titanate nanoceramics prepared via Sol-Gel method, ECS J. Solid State Sci. Technol. (2021), https://doi.org/10.1149/2162-8777/ac07f9.
[25] M.F. Shukur, M.F.Z. Kadir, Hydrogen ion conducting starch-chitosan blend based electrolyte for application in electrochemical devices, Electrochim. Acta (2015), https://doi.org/10.1016/j.electacta.2015.01.167.
[26] H.S. Oh, K.T. Nam, Invited paper: application of chitin and chitosan toward electrochemical hybrid device, Electron. Mater. Lett. (2011), https://doi.org/10.1007/s13391-011-0302-9.
[27] V. Vimala, L. Cindrella, Binder-free polymer material embedded in chitosan matrix for electrochemical energy storage devices, Chem. Phys. Lett. (2022), https://doi.org/10.1016/j.cplett.2022.140172.
[28] C. Naveen, M. Muthuvinayagam, Studies on electrical properties of Chitosan-PVA based biopolymer electrolytes for electrochemical devices, J. Polym. Res. (2023), https://doi.org/10.1007/s10965-023-03741-3.
[29] A. Rodríguez-Juárez, V. Carmona-Álvarez, F. Díaz-Monge, E. Chigo-Anota, O. Zaca-Moran, Understanding of the effect of the adsorption of atom and cluster silver on chitosan: an in silico analysis, Molecules (2023), https://doi.org/10.3390/molecules28155809.
[30] H.A. Ezzat, M.A. Hegazy, N.A. Nada, M.A. Ibrahim, Effect of nano metal oxides on the electronic properties of cellulose, chitosan and sodium alginate, Biointerface Res. Appl. Chem. (2019), https://doi.org/10.33263/BRIAC94.143149.
[31] E.S.M. El-Sayed, A. Omar, M. Ibrahim, W.I. Abdel-Fattah, On the structural analysis and electronic properties of chitosan/hydroxyapatite interaction, J. Comput. Theor. Nanosci. (2009), https://doi.org/10.1166/jctn.2009.1228.
[32] E. Fazio, et al., Nanoparticles engineering by pulsed laser ablation in liquids: concepts and applications, Nanomaterials (2020), https://doi.org/10.3390/nano10112317.
[33] D. Zhang, Z. Li, K. Sugioka, Laser ablation in liquids for nanomaterial synthesis: diversities of targets and liquids, JPhys Photonics (2021), https://doi.org/10.1088/2515-7647/ac0bfd.
[34] M. Marsico, et al., Enhancing the antibacterial properties of chitosan coatings: ag@chitosan and chitosan from insects, Coatings (Oakv.) 14 (8) (2024), https://doi.org/10.3390/coatings14080925.
[35] T.D. Dorney, R.G. Baraniuk, D.M. Mittleman, Material parameter estimation with terahertz time-domain spectroscopy, J. Opt. Soc. Am. A (2001), https://doi.org/10.1364/JOSAA.18.001562.
[36] I. Pupeza, R. Wilk, M. Koch, Highly accurate optical material parameter determination with THz time-domain spectroscopy, Opt. Express (2007), https://doi.org/10.1364/oe.15.004335.
[37] M. Scheller, C. Jansen, M. Koch, Analyzing sub-100-μm samples with transmission terahertz time domain spectroscopy, Opt. Commun. (2009), https://doi.org/10.1016/j.optcom.2008.12.061.
[38] P.N.S. Zondi Nate, Makwena justice MolotoPierre Kalenga Mubiayi, "Green synthesis of chitosan capped silver nanoparticles and their antimicrobial activity,", MRS Adv. (2018) https://doi.org/10.1557/adv.2018.368.
[39] M. Triunfo, et al., Characterization of chitin and chitosan derived from Hermetia illucens, a further step in a circular economy process, Sci. Rep. 12 (1) (2022) 1–17, https://doi.org/10.1038/s41598-022-10423-5.
[40] E. Podgorbunskikh, T. Kuskov, D. Rychkov, O. Lomovskii, A. Bychkov, Mechanical amorphization of chitosan with different molecular weights, Polymers 14 (20) (2022), https://doi.org/10.3390/polym14204438.
[41] F. Mohamed, R.A. Zaghlool, W. El Hotaby, Terahertz spectroscopic analysis of non-radiated and radiated synthetic and natural polymer/GO nanocomposites, J. Mol. Struct. (2022), https://doi.org/10.1016/j.molstruc.2021.131659.
[42] T.L. Cocker, et al., Microscopic origin of the Drude-Smith model, Phys. Rev. B (2017), https://doi.org/10.1103/PhysRevB.96.205439.
[43] K. Shimakawa, T. Itoh, H. Naito, S.O. Kasap, The origin of Non-Drude terahertz conductivity in nanomaterials, Appl. Phys. Lett. (2012), https://doi.org/10.1063/1.3697404.
[44] G. Papari, C. Koral, T. Hallam, G.S. Duesberg, A. Andreone, Terahertz spectroscopy of amorphous WSe_2 and $MoSe_2$ thin films, Materials 11 (9) (2018), https://doi.org/10.3390/ma11091613.
[45] H. Němec, P. Kužel, V. Sundström, Far-infrared response of free charge carriers localized in semiconductor nanoparticles, Phys. Rev. B Condens. Matter (2009), https://doi.org/10.1103/PhysRevB.79.115309.
[46] C.S. Yang, et al., Non-drude behavior in indium-tin-oxide nanowhiskers and thin films investigated by transmission and reflection thz time-domain spectroscopy, IEEE J. Quant. Electron. (2013), https://doi.org/10.1109/JQE.2013.2270552.
[47] N.V. Smith, Classical generalization of the drude formula for the optical conductivity, Phys. Rev. B Condens. Matter 64 (15) (2001), https://doi.org/10.1103/PhysRevB.64.155106.
[48] W.C. Chen, R.A. Marcus, The drude-smith equation and related equations for the frequency-dependent electrical conductivity of materials: insight from a memory function formalism, ChemPhysChem (2021), https://doi.org/10.1002/cphc.202100299.
[49] C. Imparato, et al., Photocatalytic hydrogen evolution by co-catalyst- -free TiO2/C bulk heterostructures synthesized under mild conditions, RSC Adv. 10 (2020) 12519–12534, https://doi.org/10.1039/D0RA01322F.
[50] C. Koral, B. Ortaç, H. Altan, Terahertz time-domain study of silver nanoparticles synthesized by laser ablation in organic liquid, IEEE Trans. Terahertz Sci. Technol. 6 (4) (2016) 525–531, https://doi.org/10.1109/TTHZ.2016.2572360.
[51] E. Prokhorov, J.G. Luna-Bárcenas, J.B. González-Campos, I.C. Sanchez, Conductivity mechanisms in a composite of chitosan-silver nanoparticles, Mol. Cryst. Liq. Cryst. (2011), https://doi.org/10.1080/15421406.2011.538327.
[52] E. Prokhorov, G. Luna-Bárcenas, J.B. González-Campos, Y. Kovalenko, Z.Y. García-Carvajal, J. Mota-Morales, Proton conductivity and relaxation properties of chitosan-acetate films, Electrochim. Acta (2016), https://doi.org/10.1016/j.electacta.2016.08.148.
[53] M.K. Hassan, A. Abukmail, A.J. Hassiba, K.A. Mauritz, A.A. Elzatahry, PVA/chitosan/silver nanoparticles electrospun nanocomposites: molecular relaxations investigated by modern broadband dielectric spectroscopy, Nanomaterials (2018), https://doi.org/10.3390/nano8110888.
[54] J. Hernández-Vargas, et al., Chitosan/MWCNTs-decorated with silver nanoparticle composites: dielectric and antibacterial characterization, J. Appl. Polym. Sci. (2014), https://doi.org/10.1002/app.40214.
[55] J.B.G. Jez-Campos, E. Prokhorov, G. Iuna-Bárcenas, A. Fonseca-García, I. C. Sanchez, Dielectric relaxations of chitosan: the effect of water on the α-relaxation and the glass transition temperature, J. Polym. Sci., Part B: Polym. Phys. (2009), https://doi.org/10.1002/polb.21823.
[56] Z. Salnikova, A. Kononov, Derivation of the Havriliak - Negami Equation for the Complex Electrical Modulus, 2020, https://doi.org/10.1063/5.0034028.
[57] G.M. Tsangaris, G.C. Psarras, N. Kouloumbi, Electric modulus and interfacial polarization in composite polymeric systems, J. Mater. Sci. (1998), https://doi.org/10.1023/A:1004398514901.
[58] Y. Zhang, W. Wang, J. Zhang, Y. Ni, Dielectric relaxation processes in PVDF composite, Polym. Test. (2020), https://doi.org/10.1016/j.polymertesting.2020.106801.
[59] T.P. Iglesias, G. Vilão, J.C.R. Reis, An approach to the interpretation of cole-Davidson and Cole-Cole dielectric functions, J. Appl. Phys. (2017), https://doi.org/10.1063/1.4985839.
[60] C. Grosse, A program for the fitting of Debye, Cole-Cole, Cole-Davidson, and Havriliak-Negami dispersions to dielectric data, J. Colloid Interface Sci. (2014), https://doi.org/10.1016/j.jcis.2013.12.031.
[61] L. Duan, J. Duan, M. Li, Relaxation functions interpolating the Cole–Cole and kohlrausch–williams–watts dielectric relaxation models, Symmetry (Basel) (2023), https://doi.org/10.3390/sym15061281.
[62] J.G. Powles, The interpretation of dielectric measurements using the cole-cole plot, Proc. Phys. Soc. (1951), https://doi.org/10.1088/0370-1301/64/1/109. Section B.
[63] J.E. Leal-Perez, et al., Cole-Cole analysis and optoelectronic properties, using VEELS, of KNNS ferroelectric ceramics, Mater. Today Commun. (2022), https://doi.org/10.1016/j.mtcomm.2022.104781.
[64] A.M. Abdullah, S.B. Aziz, S.R. Saeed, Structural and electrical properties of polyvinyl alcohol (PVA):Methyl cellulose (MC) based solid polymer blend electrolytes inserted with sodium iodide (NaI) salt, Arab. J. Chem. (2021), https://doi.org/10.1016/j.arabjc.2021.103388.

[65] D.C. Bharati, H. Kumar, A.L. Saroj, Chitosan-PEG-NaI based bio-polymer electrolytes: structural, thermal and ion dynamics studies, Mater. Res. Express (2019), https://doi.org/10.1088/2053-1591/ab66a3.

[66] V. Compañ, R. Diaz-Calleja, J. Diaz-Boils, J. Escorihuela, Distribution of relaxation times: debye length distribution vs electrode polarization by a cole−cole relaxation model, J. Electrochem. Soc. (2022), https://doi.org/10.1149/1945-7111/ac4bf9.

[67] W. Deng, I.B. Morozov, Mechanical interpretation and generalization of the Cole-Cole model in viscoelasticity, Geophysics (2018), https://doi.org/10.1190/geo2017-0821.1.

[68] S. Lucyszyn, Evaluating Surface Impedance Models for Terahertz Frequencies at Room Temperature, PIERS Online, 2007, https://doi.org/10.2529/piers061006115842.

[69] K.P. Padmasree, D.K. Kanchan, Modulus studies of CdI2-Ag2O-V2O 5-B2O3 system, Mater. Sci. Eng., B (2005), https://doi.org/10.1016/j.mseb.2005.04.011.

[70] K.P. Padmasree, D.K. Kanchan, A.R. Kulkarni, Impedance and modulus studies of the solid electrolyte system 20CdI 2-80[xAg2O-y(0.7V2O5-0.3B 2O3)], where 1 $\leq$x/y $\leq$ 3, Solid State Ionics (2006), https://doi.org/10.1016/j.ssi.2005.12.019.